FIR Filter Design Technique to Mitigate Gibb's Phenomenon

Niyan Marchon and Gourish Naik

Abstract A unique methodology employing a linear phase finite impulse response (FIR) low pass filter (LPF) was proposed with an attempt to mitigate passband and stopband ripples due to Gibb's phenomenon. The three regions of the filter response in the frequency domain are approximated using trigonometric functions. The proposed filter model achieved a sharp transition of 2π, fairly flat passband and a stopband attenuation of 40 dB. Our algorithm suppressed the oscillations near the edge of the transition region as well as in the passband region, reducing the Gibb's phenomenon from the conventional passband ripples from 18% to as low as 2%. Thus a three-fold satisfactory performance was achieved in all the three bands namely passband, transition and stopband. Our proposed linear phase FIR LPF was effectively used to filter out power line interference and higher unwanted frequencies from the real time electroencephalogram signals.

Keywords Finite impulse response · Linear phase · Low pass filter · Gibb's phenomenon · Electroencephalogram

1 Introduction

To design a finite impulse response (FIR) filter we can approximate the frequency response H (ω) of filter by calculating its impulse response h (n) [1].

$$H(\omega) = \sum_{n=-\infty}^{\infty} h(n)\, e^{-j\omega n} \tag{1}$$

N. Marchon (✉)
Padre Conceicao College of Engineering, Verna, Goa, India
e-mail: niyanmarchon@gmail.com

G. Naik
Electronics Department, Goa University, Taleigao, Goa, India

C. Shreesha and R. D. Gudi (eds.), *Control Instrumentation Systems*,
Lecture Notes in Electrical Engineering 581,
https://doi.org/10.1007/978-981-13-9419-5_10

$$h(n) = \frac{1}{2\pi} \int_{-\pi}^{\pi} H(\omega)\, e^{j\omega n} d\omega \quad -\infty \leq \mathrm{n} \leq \infty \tag{2}$$

As the duration of the impulse response is infinite and it can be truncated at n = N − 1, to obtain an FIR filter at length N as shown in Eq. (3).

$$h'(n) = \begin{cases} h(n) & n = 0, 1 \ldots N-1, \\ 0, & otherwise. \end{cases} \tag{3}$$

An oscillatory pattern or ripples are observed in the magnitude response when the impulse response coefficients of the FIR filter are truncated. The number of ripples, both in the stopband and the passband are directly proportional to the increasing of the length of the FIR filter, while there is reduction in the width of the ripples [2]. The oscillatory ripples although being narrow, the height of the ripples are constant. The maximum ripples occur at the fiduciary edges or near the transition points. This undesirable trait is called as Gibb's phenomenon [3]. This effect appears as a fixed percentage overshoot and ripple before and after the discontinuity. This is true because it is impossible to obtain an infinite slope using only a finite number of terms. As stated, as the number of terms increase, the ripples do not decrease but are squeezed into a narrower interval about the discontinuity. Even in the infinite sum, this overshooting and undershooting persists and the complete series has flanges. Resulting, the series in trying to follow the discontinuity, overshoots the mark by about 18% [4] over a region before settling down to a correct value of unity. For this reason the rectangular window is not of much practical use and other window sequences w(n) alleviate this problem as seen in Fig. 1.

The optimal method represented by various algorithms such as Chebyshev approximation criterion [5, 6], Remez exchange algorithm [7], Park McClellan algorithm [8] have been developed and works on the concept of having equiripples in the pass-

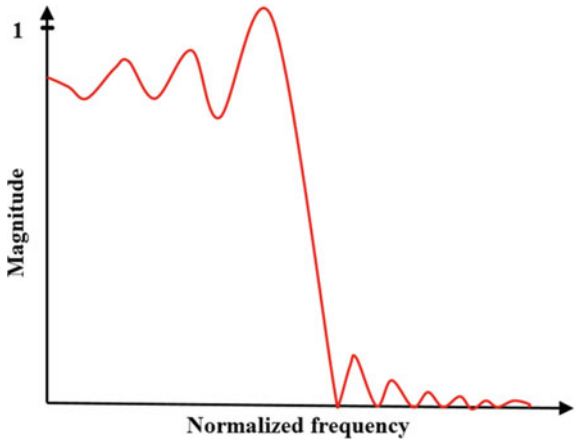

Fig. 1 Low pass filter designed with a rectangular window for a certain N

band and stopband. In the passband, the ripples oscillates between 1 − δp and 1 + δp and 0 and δs in the stopband. The main algorithm is an iterative process to determine the extremal frequencies of a filter whose amplitude frequency response satisfies the optimality condition. Algorithms such as Interpolated FIR filters [9], frequency response masking filters [10] among others FIR filter designs [11, 12] were reviewed before proposing a new technique using a linear phase low pass filter algorithm wherein the stopband, transition band and the passband regions of the filter magnitude response are modelled using trigonometric functions as it is obtained for the band pass filter design in [13]. In a similar way in [14], the sinusoidal trigonometric functions aid in computing the impulse response coefficients of the filters. In this method [14] the center frequency decides the band edges of the filter and the design parameters.

2 Proposed Methodology Using Linear Phase FIR Filter

In this section, the detailed design of the linear phase FIR low pass filter is proposed where, H (ω) is the magnitude of the filter response, δs is the stopband attenuation and δp is the passband ripple [15].

In the *passband region* of $0 \leq \omega \leq \omega_{cl}$, the frequency response is

$$H(\omega) = (1 - \delta_p) + \delta_p \cos(k_{pl}\,\omega) \tag{4}$$

$$\begin{aligned} &At\ \omega = 0; \quad H(0) = (1 - \delta_p) + \delta_p = 1 \\ &At\ \omega = \omega_{cl};\ H(\omega_{cl}) = (1 - \delta_p) + \delta_p \cos(k_{pl}\omega_{cl}) = 1 - \delta_p \\ &\therefore\ k_{pl} = \tfrac{\pi}{2\omega_{cl}} \end{aligned} \tag{5}$$

In the *sharp transition region* for $\omega_{cl} \leq \omega \leq \omega_{sl}$, the frequency response is,

$$H(\omega) = \delta_s + (1 - \delta_p - \delta_s) \cos k_{tl}(\omega - \omega_{cl}) \tag{6}$$

$$\begin{aligned} &At\ \omega = \omega_{cl};\ H(\omega_{cl}) = \delta_s + (1 - \delta_p - \delta_s) = 1 - \delta_p \\ &At\ \omega = \omega_{sl};\ H(\omega_{sl}) = \delta_s + (1 - \delta_p - \delta_s) \cos k_{tl}(\omega_{sl} - \omega_{cl}) = \delta_s \\ &\therefore\ k_{kl} = \tfrac{\pi}{2\,(\omega_{sl} - \omega_{cl})} \end{aligned} \tag{7}$$

In the *stop band region* for $\omega_{sl} \leq \omega \leq \pi$, the frequency response is,

$$H(\omega) = \delta_s - \delta_s \sin(k_{sl}(\omega - \omega_{sl})) \tag{8}$$

$$\begin{aligned} &At\ \omega = \omega_{sl};\ H(\omega_{sl}) = \delta_s - \delta_s \sin k_{sl}(\omega - \omega_{sl}) = \delta_s \\ &At\ \omega = \pi; \quad H(\pi) = \delta_s - \delta_s \sin k_{sl}(\pi - \omega_{sl}) = 0 \\ &\therefore\ k_{sl} = \tfrac{\pi}{2(\pi - \omega_{sl})} \end{aligned} \tag{9}$$

Passband (k_{pl}), transition (k_{tl}) and stopband (k_{sl}) are filter design parameters derived in Eqs. (5), (7) and (9) respectively.

2.1 Expressions for Impulse Response Coefficients for the FIR LPF

The impulse response coefficients h (n) for the FIR LPF are obtained by computing the integral limits of the three regions of the filter magnitude response.

$$h(n) = \frac{1}{\pi}\left\{\int_0^{\omega_{cl}} H(\omega)\cos k\,\omega\,\partial\omega + \int_{\omega_{cl}}^{\omega_{sl}} H(\omega)\cos k\,\omega\,\partial\omega + \int_{\omega_{sl}}^{\pi} H(\omega)\cos k\,\omega\,\partial\omega\right\} \tag{10}$$

Solving the 1st term from Eq. (10)

$$1\text{st term} = h_{1l}(n) = \frac{1}{\pi}\int_0^{\omega_{cl}} \left[(1-\delta_p) + \delta_p \cos k_{pl}\omega\right]\cos k\,\omega\,\partial\omega$$

$$= \frac{(1-\delta_p)\sin k\omega_{cl}}{k\pi} + \frac{\delta_p}{\pi\left(k_{pl^2} - k^2\right)}\left[k_{pl}\sin\left(k_p r\omega_{cl}\right)\cos(k\omega_{cl}) - k\cos\left(k_{pl}\omega_{cl}\right)\sin(k\omega_{cl})\right] \tag{11}$$

Solving the 2nd term from Eq. (10)

$$2\text{nd term} = h_2(n) = \frac{1}{\pi}\int_{\omega_{cl}}^{\omega_{sl}} \left[\delta_s + \left(1-\delta_p-\delta_s\right)\cos\ k_{tl}(\omega-\omega_{cl})\right]\cos\ k\omega\,\partial\omega$$

$$= \frac{\delta_s}{k\pi}[\sin k\omega_{sl} - \sin k\omega_{cl}]$$

$$+ \frac{\left(1-\delta_p-\delta_s\right)}{\pi\left(ktl^2 - k^2\right)}\begin{bmatrix} k_{tl}\sin k_{tl}(\omega_{sl}-\omega_{cl})\cos(k\omega_{sl}) - k\cos k_{tl}(\omega_{sl}-\omega_{cl})\sin(k\omega_{sl}) \\ +k\sin(k\omega_{cl}) \end{bmatrix} \tag{12}$$

Solving the 3rd term from Eq. (10)

$$3\text{rd term} = h_3(n) = \frac{1}{\pi}\int_{\omega_{sl}}^{\pi} [\delta_s - \delta_s\sin(ksl(\omega-\omega_{sl}))]\cos k\omega\,\partial\omega$$

$$= \frac{\delta_s}{k\pi}[\sin k\,\pi - \sin k\omega_{sl}] + \frac{\delta_s}{\pi\left(k_{sl}^2 - k^2\right)}$$

$$[k_{sl}\cos[(k_{sl}(\pi-\omega_{sl})]\cos k\,\pi + k\sin[(k_{sl}(\pi-\omega_{sl})]\sin k\,\pi - k_{sl}\cos(k\omega_{sl})] \tag{13}$$

By substituting Eqs. (11)–(13) in Eq. (10) we obtain the expression for the low pass filter impulse response h (n). Where $k \neq k_{tl}$, k_{pl} *and* k_{sl}.

$$
\begin{aligned}
h(n) = & \left\{ \left(\frac{\delta_s}{k\pi} \right) \left[\sin(k\omega_{sl}) - \sin(k\omega_{cl}) + \sin(k\pi) - \sin(k\omega_{sl}) \right] + \frac{(1-\delta_p)\sin(k\omega_{cl})}{k\pi} \right\} \\
& + \left\{ \left(\frac{\delta_p}{\pi\left(k_{pl}^2 - k^2\right)} \right) \left[k_{pl} \sin(k_p r\omega_{cl}) \cos(k\omega_{cl}) - k \cos\left(k_{pl}\omega_{cl}\right) \sin(k\omega_{cl}) \right] \right\} \\
& + \left\{ \left(\frac{(1-\delta_p-\delta_s)}{\pi(ktl^2 - k^2)} \right) \left[k \sin(k\omega_{cl}) + k_{tl} \sin(k_{tl}(\omega_{sl} - \omega_{cl})) \cos(k\omega_{sl}) - k \cos(ktt(\omega_{sl} - \omega_{cl})) \sin(k\omega_{sl}) \right] \right\} \\
& + \left\{ \left(\frac{\delta_s}{\pi\left(k_{sl}^2 - k^2\right)} \right) \left[k_{sl} \cos(k_{sl}(\pi - \omega_{sl})) \cos(k\pi) + k \sin(k_{sl}(\pi - \omega_{sl})) \sin(k\pi) - k_{sl} \cos(k\omega_{sl}) \right] \right\} \qquad (14)
\end{aligned}
$$

Equation (14) is the expression for the LPF model impulse response h(n).

2.2 *Expression for the Frequency Response of the FIR Low Pass Filter*

We selected the symmetric impulse response, h(n) = h(N − 1 − n) for N Even and the appropriate type of frequency response for the linear phase FIR LPF as shown below [1, 4].

$$H_r(\omega) = 2 \sum_{n=0}^{\left(\frac{N}{2}\right)-1} h(n) \cos\left(\omega \left(\frac{N-1}{2} - n \right) \right) \qquad (15)$$

This filter design is most suitable for LPFs as the H(0) gives a maximum value, while H(π) = 0.

3 Results

The performance of the FIR low pass filter for various filter orders (N) are clearly depicted in Fig. 2. Where in the passband loss is as low as 6.34% for N = 200 and further reduces to nearly 2% at larger filter order (N = 2000). There is a reduction of Gibb's phenomenon with our proposed linear phase FIR LPF designs. As we know the conventional FIR filters, the peak passband ripple due to Gibb's phenomenon is about 18%, our passband loss is very much low as compared to the conventional peak passband ripple value. Using our proposed low pass FIR filters, we also observed from Figs. 3 and 4, that (i) the passband losses are quite low, (ii) The ripple decreases for higher filter order and (iii) The filter exhibited sharp transition region as low of 2π. The magnitude response for various filter orders ranging from N = 200 to N =

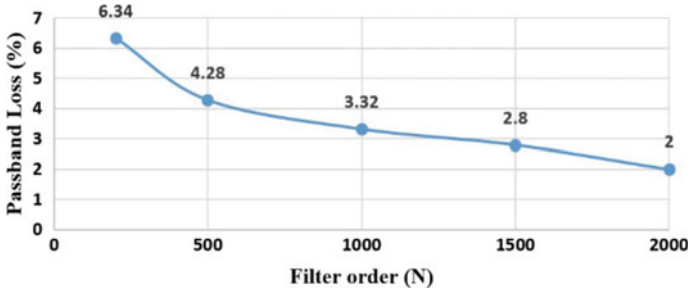

Fig. 2 Passband loss of the LPF design for various filter order

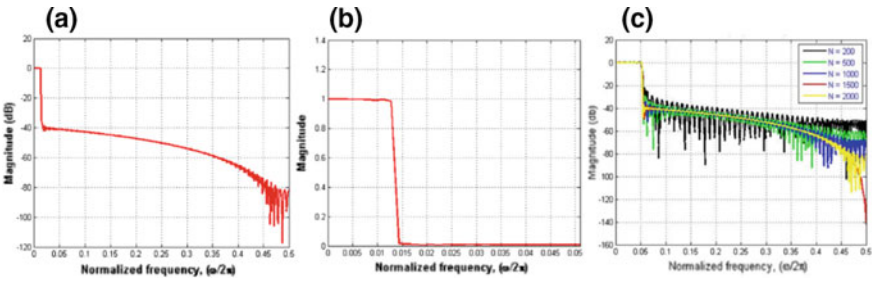

Fig. 3 Linear phase FIR LPF **a** magnitude response (N = 1000) **b** linear plot (N = 1000) **c** magnitude response for various filter order

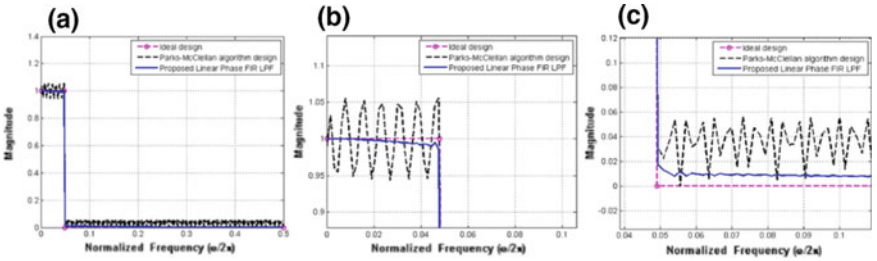

Fig. 4 Magnitude response of PM algorithm as compared with the proposed LPF **a** linear plot **b** magnified pass band view **c** magnified stopband view

2000 were also plotted to evaluate the performance of the proposed LPF as shown in Fig. 3c. These filters are unlike the classical filters, possess a narrow stopband and/or passband. The stopband attenuation was recorded to be 40 dB. The proposed design was compared with the optimal linear phase FIR method such as the Parks McClellan (PM) algorithm. The PM algorithm exhibits large ripple in the pass and the stop bands as compared to our proposed algorithm as shown in Fig. 4a–c.

The proposed linear phase FIR LPF was used to filter an electroencephalogram (EEG) signal whose recording was taken for a single subject (activity: relaxed and alert) for a duration of 5 min. As many as 20 EEG channels were collected with

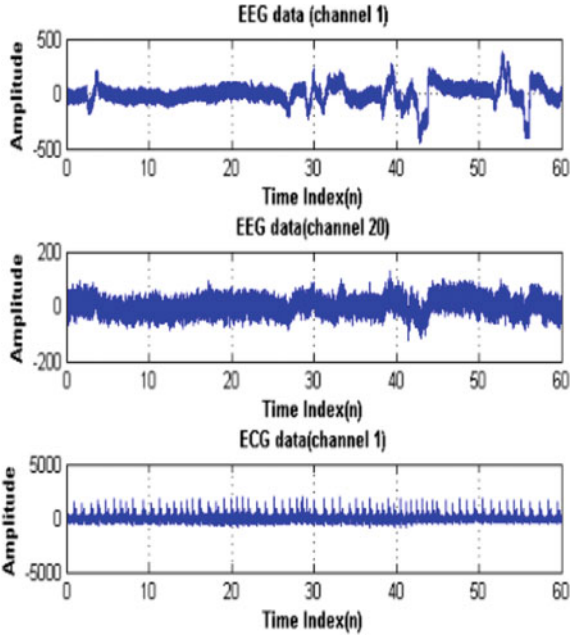

Fig. 5 Real time EEG signals from a healthy subject

the sampling frequency (fs) of 256 Hz. To enable and filter in the Theta–Alpha frequencies from the raw EEG signal [16–18], the sharp transition capable linear phase FIR LPF set its passband edge to 12 Hz and the stopband edge at 13 Hz. Figure 5 shows the extracted real time EEG signal from the subject from channel 1 and 20 (other channel signals are not shown here). Figure 6a displays the FFT spectrum of the original EEG (in blue) and the FFT of the filtered EEG after using our proposed FIR filter (in red). The high frequency artifacts, frequencies above

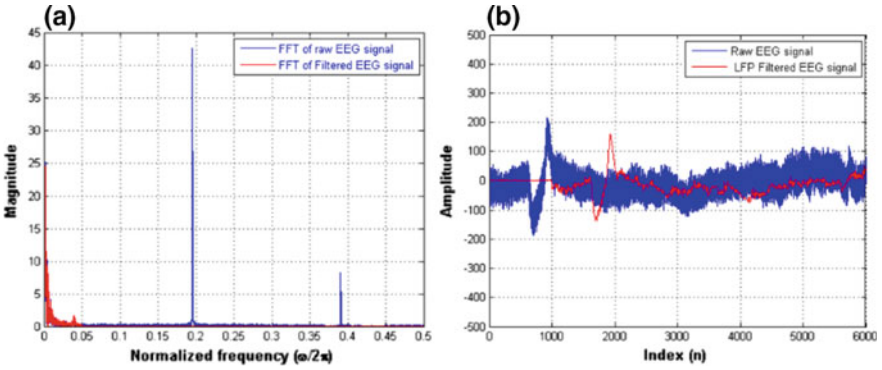

Fig. 6 Real time EEG signal along with filtered EEG signal **a** frequency domain **b** time domain

13 and 50 Hz power line interference (PLI) and its harmonics are also filtered and suppressed. The time domain traces in Fig. 6b displays the original EEG signal (in blue) and the noise free EEG signal (shown in red) which can be further analyzed and processed.

4 Conclusions

Using the trigonometric functions of frequency the impulse response coefficients are computed for the three regions of the filter response in the frequency domain. The proposed filter model stressed on achieving a sharp transition and a flat passband. As the filter gets sharper in the transition region, more oscillations or ripples will be the frequency response near the edge of the passband, a trait described as Gibb's phenomenon. However our proposed filter model achieved a fair trade-off between the transition bandwidth and the Gibb's phenomenon. Using our methodology, a low passband ripple of 2% was achieved for filter order 2000 with a stopband attenuation of 40 dB. It was also seen that our proposed method had a flat passband and stopband as compared to the large ripples seen in the passband and stopband bands using the Parks McClellan algorithm Thus a threefold satisfactory performance was achieved in all the three bands namely passband, transition and stopband. Our proposed linear phase FIR LPF was effectively used to filter out PLI and higher unwanted high frequencies from the real time EEG signals with sharp transition filter band edges.

Acknowledgements The authors would like to thank Mr. Noel Tavares, research scholar from the Electronics department, Goa University for collecting the EEG clinical data for testing our filter algorithm.

References

1. Ifeachor EC, Jervis BW (2002) Digital signal processing: a practical approach. Pearson Education, pp 367–379
2. Proakis JG, Manolakis DG (1992) Digital signal processing-principles, algorithms and applications
3. Gibbs AJ (1970) The design of digital filters in Australian. Telecommun Res J 4:29–34
4. Johnson JR (1989) Introduction to digital signal processing. Prentice Hall, Englewood Cliffs, NJ, pp 426-440
5. Rabiner LR et al (1975) FIR digital filter design techniques using weighted Chebyshev approximation. Proc IEEE 63(4):595–610
6. Alkhairy A et al (1991) Design of FIR filters by complex Chebyshev approximation. In: IEEE international conference on acoustics, speech, and signal processing, ICASSP-91, pp 1985–1988
7. Saramäki T, Lim YC (2003) Use of the Remez algorithm for designing FRM based FIR filters. Circ Syst Signal Process 22(2):77–97
8. Vaidyanathan P (1985) Optimal design of linear phase FIR digital filters with very flat passbands and equiripple stopbands. IEEE Trans Circuits Syst 32(9):904–917

9. Saramaki T et al (1988) Design of computationally efficient interpolated FIR filters. IEEE Trans Circ Syst 35(1):70–88
10. Lim Y (1986) Frequency-response masking approach for the synthesis of sharp linear phase digital filters. IEEE Trans Circ Syst 33(4):357–364
11. Jing Z, Fam A (1984) A new structure for narrow transition band, low pass digital filter design. IEEE Trans Acoust Speech Signal Process 32(2):362–370
12. Henzel N, Leski JM (2013) Generalized constraint design of linear-phase FIR digital filters. In: Proceedings of the 8th international conference on computer recognition systems CORES 2013. Springer, Heidelberg, pp 53–62
13. Marchon N et al (2018) Linear phase sharp transition BPF to detect noninvasive maternal and fetal heart rate. J Healthc Eng Hindawi 2018:1–14
14. Rodrigues J, Pai KR (2005) New approach to the synthesis of sharp transition FIR digital filter. In: Proceedings of the IEEE international symposium industrial electronics, vol 3, pp 1171–1173
15. Marchon N et al (2018) Monitoring of fetal heart rate using sharp transition FIR filter. Biomed Signal Process Control 44:191–199
16. Britton JW et al (2016) Electroencephalography (EEG): an introductory text and atlas of normal and abnormal findings in adults, children, and infants. American Epilepsy Society, Chicago
17. Akiyama M et al (2017) Theta-alpha EEG phase distributions in the frontal area for dissociation of visual and auditory working memory. Sci Rep 7:42776
18. Malmivuo J, Plonsey R (1995) Bioelectromagnetism: principles and applications of bioelectric and biomagnetic fields. Oxford University Press, USA